Two-Dimensional Electron-Photon Systems in Periodic Nanostructures under External Magnetic Fields

Vram Mughnetsyan,

Center for Modeling and Simulations
of Nanostructures (**NanoSM**),
Laboratory of Solid State Physics,
Yerevan State University,
1 Al. Manoogian, 0025, Yerevan, Armenia,
Tel: +374 93 245700
Email: vram@ysu.am, vrammugh@gmail.com

Published articles: ***1 Physical Review B, (Q1)***
1 Annalen der Physik, (Q2)

Under review: ***1 Physics Letters A (Q2)***
1 Physica B (Q2)

Submitted: ***1 Physical Review B, (Q1)***

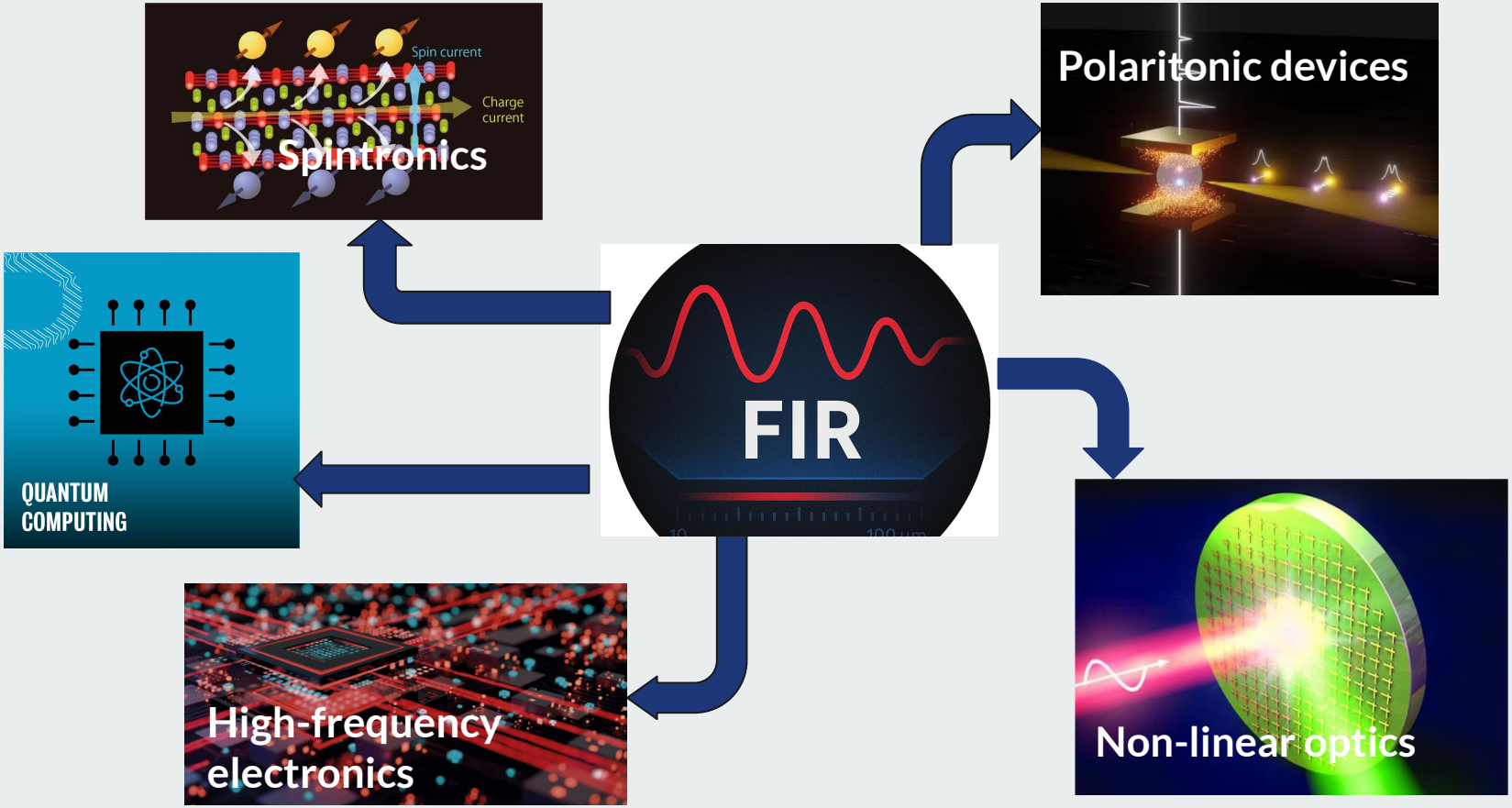
Spin current
Charge current
Spintronics
Polaritonic devices
QUANTUM COMPUTING
FIR
High-frequency electronics
Non-linear optics

PHYSICAL REVIEW B VOLUME 54, NUMBER 24 15 DECEMBER 1996-II

Long-mean-free-path ballistic hot electrons in high-purity GaAs

B. Brill and M. Heiblum
Braun Center for Submicron Research, Department of Condensed Matter Physics, Weizmann Institute of Science, Rehovot 76100, Israel
(Received 18 July 1996)

The mean free path (mfp) of hot ballistic electrons, injected into high-purity GaAs, was measured and found to be several micrometers long. The hot electrons were injected at energies just below the LO-phonon emission threshold and their mfp was measured by two techniques: first, by comparing different devices with different layer thickness; and second, in a single device, utilizing the cyclotron motion of ballistic electrons in tilted magnetic fields. We find the mfp scales roughly inversely with impurity concentration. We suggest that the dominant scattering is due to impact ionization of neutral impurities. [S0163-1829(96)52348-9]

Two-dimensional electron systems, with their long mean free path (mfp), have been intensively exploited for the study of ballistic and coherent effects. However, the mfp in these systems drops sharply, due to electron-electron (e-e) interactions, as either the electron's excess energy or the temperature increases (even only to 1–2 meV).[1] Alternatively, high-purity bulk GaAs may present a medium which supports long mfp ballistic transport of *hot electrons*. In lightly doped GaAs, at low enough temperatures, the bulk electrons are trapped by their parent donors (*frozen*), neutralizing them and thus minimizing both e-e and ionized impurity scattering. Since acoustical phonon scattering in GaAs is very weak, injecting electrons below the threshold for LO-phonon emission (36 meV in GaAs) may lead to a *free* motion of hot electrons with extremely long mfp ($\gtrsim 1$ μm). In this paper we study the mfp of hot electrons injected into high-purity GaAs at low temperatures. Two methods are being employed in order to measure the mfp: the first relies on comparing the transmission in several devices, each with a different layer thickness; and the second utilizes the cyclotron motion performed by the ballistic electrons around a tilted magnetic field. Since the path length depends on the tilt angle the mfp can be measured with a *single* device.

centration and the mobility as a function of temperature allows one to extract both N_D and N_A. We obtained a peak mobility of some 23 m^2/V sec (around 40 K for $N_D \cong 3 \times 10^{14}$, $N_A \cong 1 \times 10^{14}$), which is comparable to the best published data for molecular-beam-epitaxy (MBE) -grown GaAs layers. The layers were fabricated into three terminal devices using previously developed lithographic techniques.[3]

The differential transfer ratio, $\alpha = dI_c/dI_{inj}$, where I_c and I_{inj} are the collected and injected currents, respectively, measures the probability of electrons to pass the drift region without significant scattering. In order to measure the mfp of the hot electrons we fabricated several devices with the same parameters but with different drift region thickness[6] and measured the differential transfer ratio below the threshold for longitudinal optical (LO) phonon emission (36 meV) at 4.2 K. The transfer ratio was found to scale exponentially with length as seen in Fig. 2, $\alpha = \alpha_0 e^{-L/\mathrm{mfp}}$, with mfp=0.7 μm for total impurity concentration $N_D + N_A \approx 3 \times 10^{15}$ cm^{-3}. Extrapolating the drift region length to zero leads to $\alpha_0 \approx 0.7$, indicating that some 30% of the electrons are being scattered by the doped base. Applying a longitudinal magnetic field (in the direction of the growth) we found a monotonous increase in the collected current and in the mfp. At

Shubnikov–de Haas Oscillations

Ballistic transport

Aharonov–Bohm oscillations and

Persistent currents

Exciton–polariton condensation in GaAs microcavities

Coherent spin precession and long spin relaxation times ...

- **Low-temperature, high-purity GaAs**: $\lambda \sim 1 - 10$ μm
- **Moderately doped GaAs (e.g., $10^{16} - 10^{17}$ cm^{-3})**: $\lambda \sim 100 - 500$ nm
- **Heavily doped GaAs ($> 10^{18}$ cm^{-3})**: $\lambda \sim 10 - 50$ nm

nature physics

LETTERS

PUBLISHED ONLINE: 22 AUGUST 2016 | DOI: 10.1038/NPHYS3850

Collective non-perturbative coupling of 2D electrons with high-quality-factor terahertz cavity photons

Qi Zhang[1], Minhan Lou[1], Xinwei Li[1], John L. Reno[2], Wei Pan[3], John D. Watson[4], Michael J. Manfra[4,5] and Junichiro Kono[1,6,7]*

The collective interaction of electrons with light in a high-quality-factor cavity is expected to reveal new quantum phenomena[1–7] and find applications in quantum-enabled technologies[8,9]. However, combining a long electronic coherence time, a large dipole moment, and a high quality-factor has proved difficult[10–13]. Here, we achieved these conditions simultaneously in a two-dimensional electron gas in a high-quality-factor terahertz cavity in a magnetic field. The vacuum Rabi splitting of cyclotron resonance exhibited a square-root dependence on the electron density, evidencing collective interaction. This splitting extended even where the detuning is larger than the resonance frequency. Furthermore, we observed a peak shift due to the normally negligible diamagnetic term in the Hamiltonian. Finally, the high-quality-factor cavity suppressed superradiant cyclotron resonance decay, revealing a narrow intrinsic linewidth of 5.6 GHz. High-quality-factor terahertz cavities will enable new experiments bridging the traditional disciplines of condensed-matter physics and cavity-based quantum optics.

nonresonant matter decay rate, which is usually the decoherence rate in the case of solids. Strong coupling is achieved when the splitting, $2g$, is much larger than the linewidth, $(\kappa+\gamma)/2$, and ultrastrong coupling is achieved when g becomes a considerable fraction of ω_0. The two standard figures of merit to measure the coupling strength are $C \equiv 4g^2/(\kappa\gamma)$ and g/ω_0; here, C is called the cooperativity parameter[18], which is also the determining factor for the onset of optical bistability through resonant absorption saturation[20]. To maximize C and g/ω_0, one should construct a cavity QED set-up that combines a large dipole moment (that is, large g), a small decoherence rate (that is, small γ), a large cavity Q factor (that is, small κ), and a small resonance frequency ω_0.

Group III–V semiconductor quantum wells (QWs) provide one of the cleanest and most tunable solid-state environments with quantum-designable optical properties. Microcavity QW-exciton-polaritons represent a landmark realization of a strongly coupled light–condensed-matter system that exhibits a rich variety of coherent many-body phenomena[21]. However, the large values of ω_0 and relatively small dipole moments for interband transitions make it

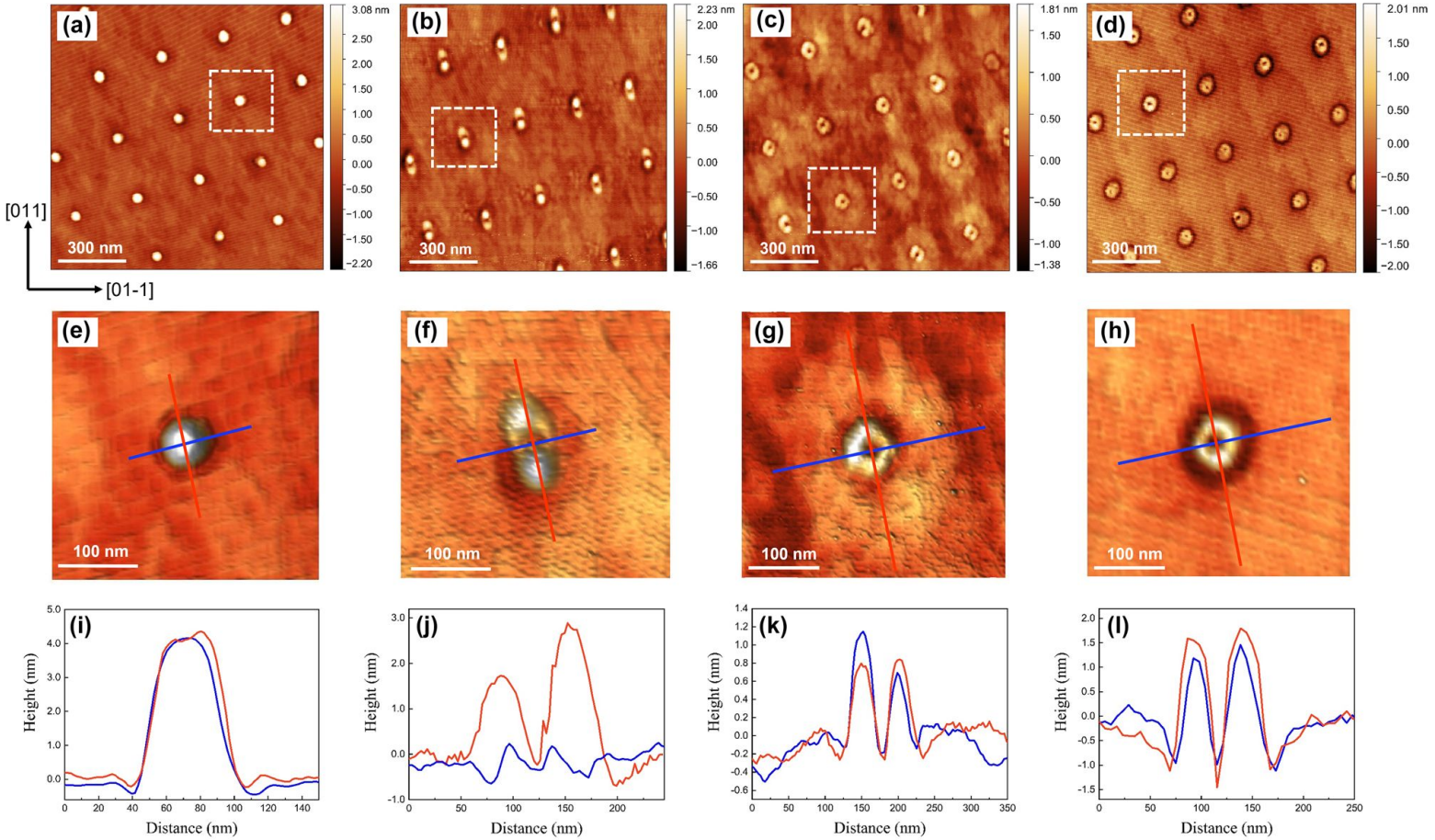
(a)
(b)
(c)
(d)
300 nm
[011]
[01-1]
3.08 nm
2.23 nm
1.81 nm
2.01 nm
(e)
(f)
(g)
(h)
100 nm
(i)
(j)
(k)
(l)
Height (nm)
Distance (nm)

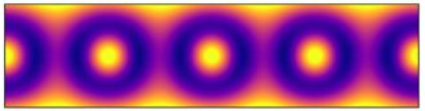

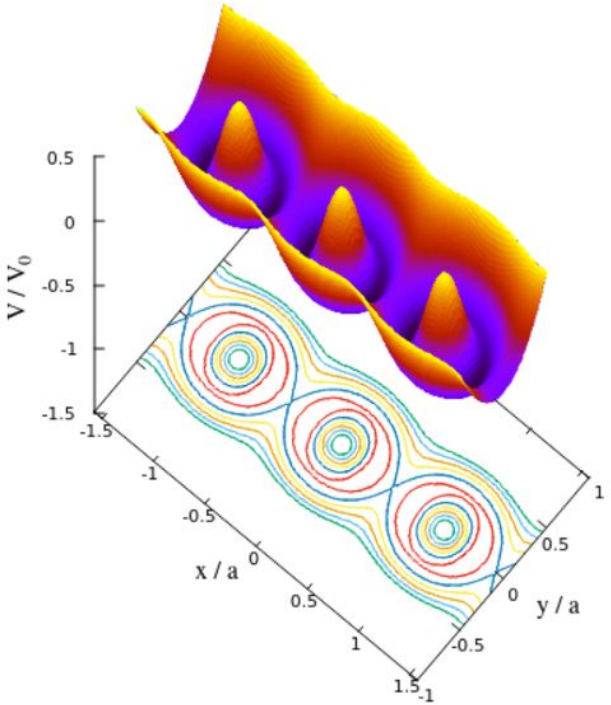

Figure 1. (Color on-line) The quantum ring chain (upper panel) and its modulation potential profile (lower panel) according to Equation (1) for the following values of parameters: $\nu_1 = 1$, $\nu_2 = 1.5$, $\nu_3 = 0.05$, $\gamma_1 = 0.15$, $\gamma_2 = 0.45$.

Armen Harutyunyan, Vram Mughnetsyan, Albert Kirakosyan, and Vidar Gudmundsson, "Magneto-Optical Properties of Electron Gas in a Chain of Planar Quantum Rings: Effect of Screening on the Signature of Quantum Phase Interference"Ann. Phys. (Berlin) 537, 2400337 (2025).

$$V_{\text{ext}}(x,y) = V_0\left[-\nu_1 \cdot \cos^2(gx/2)\exp\left(-\gamma_1(gy)^2\right) + \nu_2 \cdot \cos^4(gx/2)\exp\left(-\gamma_2(gy)^2\right) + \nu_3 \cdot (gy)^2\right]$$

$$\nu_{\text{ext}}(G,y) = V_0\left\{-\nu_1 e^{-\gamma_1(gy)^2} \cdot \frac{1}{4}(2\delta_{nx,0} + \delta_{nx,1} + \delta_{nx,-1}) + \nu_2 e^{-\gamma_2(gy)^2} \cdot \frac{1}{4}\left(\frac{3}{2}\delta_{nx,0} + \delta_{nx,1} + \delta_{nx,-1} + \frac{\delta_{nx,2} + \delta_{nx,-2}}{4}\right) + \nu_3(gy)^2 \cdot \delta_{nx,0}\right\},$$

$$V_{\text{H}}(\vec{r}) = \frac{e^2}{\varkappa}\int_{\mathbb{R}^2} \frac{\Delta n(\vec{r}')}{|\vec{r} - \vec{r}'|} d\vec{r}'$$

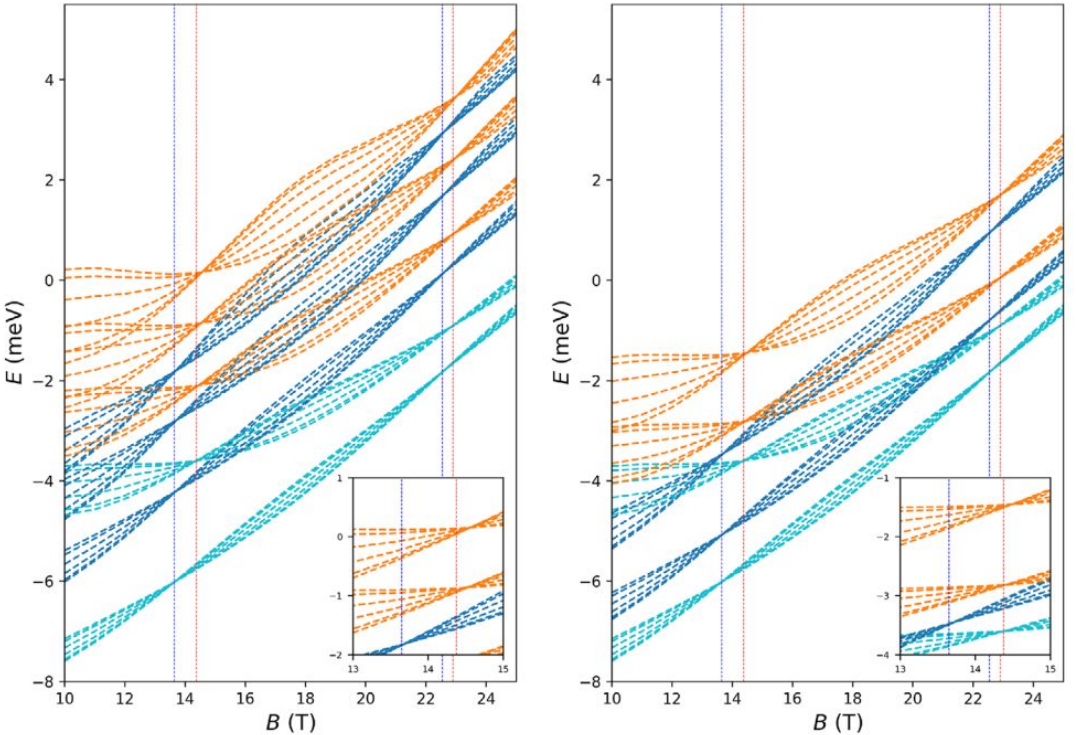

$$\Delta\phi = ka + (e/\hbar c)\int \vec{A}d\vec{l},$$

$$\Delta\phi = 2\pi n$$

$$ka - \langle y\rangle a/l_B^2 = 2\pi n,$$

Figure 4. The lowest two miniband energies for spin-up states as functions of the magnetic field for integer (left panel) and half an integer (right panel) numbers of electrons per unit cell. The light-blue dotted lines correspond to noninteracting electrons.

Only Spin-Up states

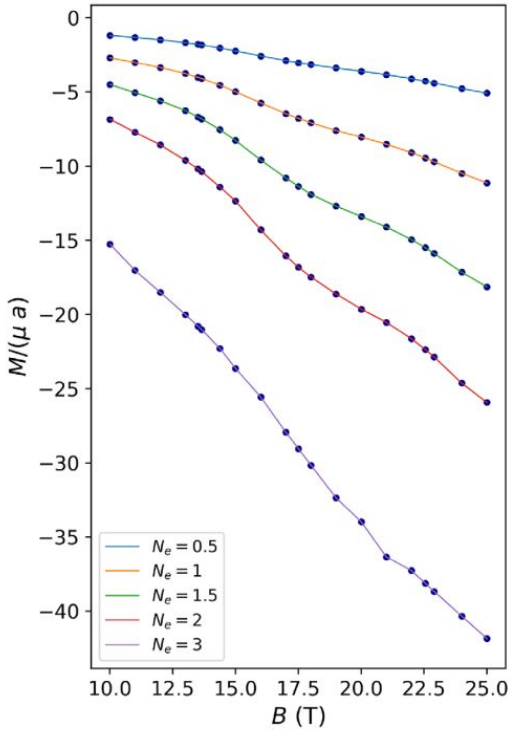

Figure 7. Dependence of the QR chain magnetization (for a UC in the units of the effective Bohr magneton) on the magnetic field induction for different numbers of electrons per a UC.

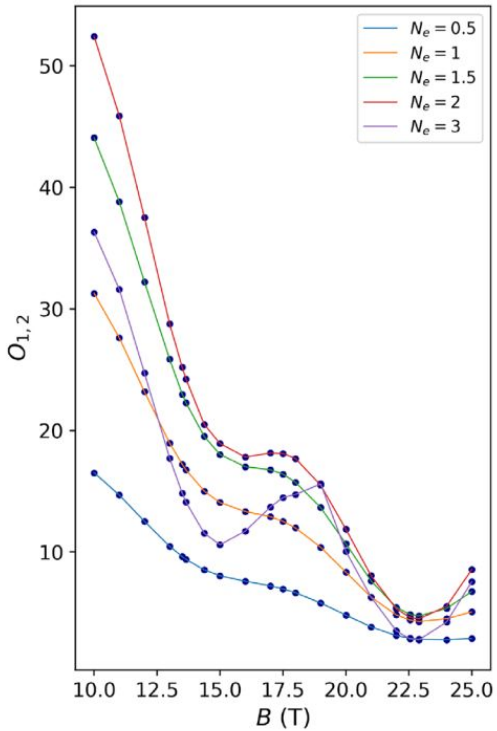

Figure 8. Dependence of the oscillator strength between the first and the second minibands of the QR chain on the magnetic field induction for different numbers of electrons per a UC.

$$O_{1,2} = \frac{a^2}{(2\pi)^2} \sum_{s_1,s_2} \int_{-\frac{\pi}{a}}^{\frac{\pi}{a}} dk_1 dk_2 O_{1,2}(k_1, k_2, s_1, s_2) \times f_{\mathrm{FD}}(E(1, s_1, k_1))(1 - f_{\mathrm{FD}}(E(2, s_2, k_2))),$$

$$O_{1,2}(k_1, k_2, s_1, s_2) = \frac{2m(E(2, s_2, k_2) - E(1, s_1, k_1))}{3\hbar^2} \times |\langle 2, k_2|\vec{r}|1, k_1\rangle|^2$$

$$\langle M \rangle = \frac{1}{2ca} \int_{UC} (\vec{r} \times \langle \vec{j}_{n,k}(\vec{r}) \rangle) d^2 r$$

Vidar Gudmundsson, Vram Mughnetsyan, Hsi-Sheng Goan, Jeng-Da Chai, Nzar Rauf Abdullah, Chi-Shung Tang, Valeriu Moldoveanu, and Andrei Manolescu, "Spin-phase transition in an array of quantum rings controlled by cavity photons", *Phys. Rev. B. 111, 115304 (2025).*

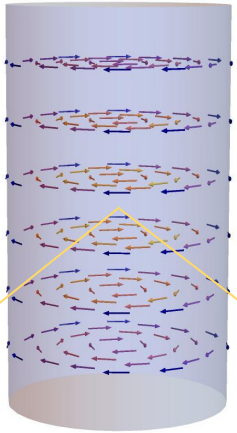

TE011

$$H_z(r,\phi,z) = B_{mnp} J_m\left(\frac{\chi'_{mn} r}{a}\right)\cos(m\phi)\sin\left(\frac{\pi p z}{d}\right)$$

$$E_\phi = -B_{011} J_1\left(\frac{\chi'_{01} r}{a}\right)\sin\left(\frac{\pi z}{d}\right)\frac{i\omega_{011}\mu}{h^2}$$

$$\hbar\omega_{011} = \hbar c\sqrt{\left(\frac{\chi'_{01}}{a}\right)^2 + \left(\frac{\pi}{d}\right)^2}.$$

$$h^2 = \omega_{011}^2 \mu\kappa - (\pi/d)^2$$

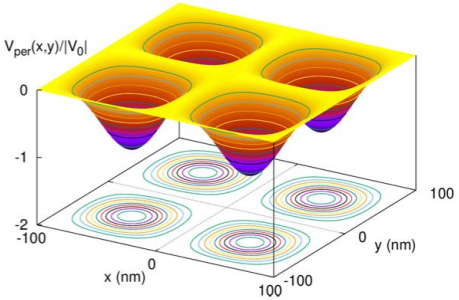

$V_0 = 16.0$ meV

$$V_{\text{per}}(\boldsymbol{r}) = -V_0\left[\sin\left(\frac{g_1 x}{2}\right)\sin\left(\frac{g_2 y}{2}\right)\right]^2$$

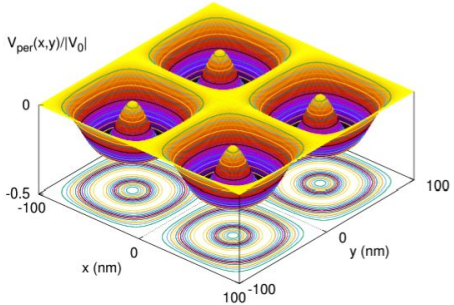

$V_0 = 64.0$ meV

$$V_{\text{per}}(\boldsymbol{r}) = -V_0\left[\sin\left(\frac{g_1 x}{2}\right)\sin\left(\frac{g_2 y}{2}\right)\right]^2 + V_0\left[\sin\left(\frac{g_1 x}{2}\right)\sin\left(\frac{g_2 y}{2}\right)\right]^4$$

Simple Exchange-Correlation Energy Functionals for Strongly Coupled Light-Matter Systems Based on the Fluctuation-Dissipation Theorem

PDF

Share

Johannes Flick [1,2,3]

Show more

Phys. Rev. Lett. **129**, 143201 – **Published 30 September, 2022**

DOI: https://doi.org/10.1103/PhysRevLett.129.143201

Export Citation

Altmetric score 9 Citations 23 Show metrics

Abstract

Recent experimental advances in strongly coupled light-matter systems have sparked the development of general *ab initio* methods capable of describing interacting light-matter systems from first principles. One of these methods, quantum-electrodynamical density-functional theory (QEDFT), promises computationally efficient calculations for large correlated light-matter systems with the quality of the calculation depending on the underlying approximation for the exchange-correlation functional. So far no true density-functional approximation has been introduced limiting the efficient application of the theory. In this Letter, we introduce the first gradient-based density functional for the QEDFT exchange-correlation energy derived from the adiabatic-connection fluctuation-dissipation theorem. We benchmark this simple-to-implement approximation on small systems in optical cavities and demonstrate its relatively low computational costs for fullerene molecules up to C_{180} coupled to 400 000 photon modes in a dissipative optical cavity. This Letter now makes first principle calculations of much larger systems possible within the QEDFT framework effectively combining quantum optics with large-scale electronic structure theory.

The Journal of Chemical Physics ARTICLE scitation.org/journal/jcp

Real-space, real-time approach to quantum-electrodynamical time-dependent density functional theory

Cite as: J. Chem. Phys. 157, 194106 (2022); doi: 10.1063/5.0123909
Submitted: 1 September 2022 • Accepted: 4 November 2022 •
Published Online: 16 November 2022

View Online Export Citation CrossMark

Justin Malave,[1] Alexander Ahrens,[1] Daniel Pitagora,[1] Cody Covington,[2] and Kálmán Varga[1,a)]

AFFILIATIONS

[1] Department of Physics and Astronomy, Vanderbilt University, Nashville, Tennessee 37235, USA
[2] Department of Chemistry, Austin Peay State University, Clarksville, Tennessee 37044, USA

[a)] **Author to whom correspondence should be addressed:** kalman.varga@vanderbilt.edu

ABSTRACT

The quantum-electrodynamical time-dependent density functional theory equations are solved by time propagating the wave function on a tensor product of a Fock-space and real-space grid. Applications for molecules in cavities show the accuracy of the approach. Examples include the coupling strength and light frequency dependence of the energies, wave functions, optical absorption spectra, and Rabi splitting magnitudes in cavities, as well as a description of high harmonic generation in cavities.

QEDFT

J. Flick, Phys. Rev. Lett. 129, 143201 (2022).

QED - DFT - TP

J. Malave, et al., J. Chem. Phys. 157, 194106 (2022).

LSDFT

B. Tanatar and D. M. Ceperley, Phys. Rev. B 39, 5005 (1989).
U. von Barth and L. Hedin, J. Phys. C 5, 1629 (1972).
J. P. Perdew and A. Zunger, Phys. Rev. B 23, 5048 (1981).

$$|\boldsymbol{\alpha}\boldsymbol{\theta}\sigma n\rangle = |\boldsymbol{\alpha}\boldsymbol{\theta}\sigma\rangle \otimes |n\rangle$$

Hamiltonian of the 2DEG-cavity system:

$$H = H_e + H_{\text{int}} + H_\gamma$$

Electronic part:

$$H_e = H_0 + H_{\text{Zee}} + V_H + V_{\text{per}} + V_{\text{xc}}$$

Kinetic energy in magnetic field:

$$H_0 = \frac{1}{2m^*}\boldsymbol{\pi}^2, \quad \text{with} \quad \boldsymbol{\pi} = \left(\mathbf{p} + \frac{e}{c}\mathbf{A}\right)$$

Spin Zeeman energy:

$$H_{\text{Zee}} = \pm g^* \mu_B^* B/2$$

Hartree potential (direct Coulomb interaction):

$$V_H(\mathbf{r}) = \frac{e^2}{\kappa}\int_{\mathbb{R}^2} d\mathbf{r}' \, \frac{\Delta n(\mathbf{r}')}{|\mathbf{r} - \mathbf{r}'|}$$

Periodic potential:

$$V_{\text{per}}(\mathbf{r}) = -V_0 \left[\sin\left(\frac{g_1 x}{2}\right)\sin\left(\frac{g_2 y}{2}\right)\right]^2$$

Electron-photon interaction:

$$H_{\text{int}} = \frac{1}{c}\int_{\mathbb{R}^2} d\mathbf{r}\, \mathbf{J}(\mathbf{r}) \cdot \mathbf{A}_\gamma(\mathbf{r}) + \frac{e^2}{2m^* c}\int_{\mathbb{R}^2} d\mathbf{r}\, n_e(\mathbf{r}) A_\gamma^2(\mathbf{r})$$

Long wavelength approximation

$$\longrightarrow \quad \boldsymbol{A}_\gamma(\boldsymbol{r}) = \boldsymbol{e}_\phi \mathcal{A}_\gamma (a_\gamma^\dagger + a_\gamma)\left(\frac{r}{l}\right)$$

$$H_{\text{int}} = g_\gamma \hbar\omega_c \{lI_x + lI_y\}(a_\gamma^\dagger + a_\gamma) + g_\gamma^2 \hbar\omega_c \mathcal{N}\left\{\left(a_\gamma^\dagger a_\gamma + \tfrac{1}{2}\right) + \tfrac{1}{2}(a_\gamma^\dagger a_\gamma^\dagger + a_\gamma a_\gamma)\right\}$$

$$l(I_x + I_y) = \frac{m^*}{e}\int_{\mathcal{A}} d\boldsymbol{x}\, \frac{l}{\hbar}\left[-J_x(\boldsymbol{x})\left(\frac{y}{l}\right) + J_y(\boldsymbol{x})\left(\frac{x}{l}\right)\right]$$

$$\mathcal{N} = \int_{\mathcal{A}} d\boldsymbol{x}\, n_{\text{e}}(\boldsymbol{x})\left(\frac{x^2 + y^2}{l^2}\right)$$

$$g_\gamma = \left\{\left(\frac{e\mathcal{A}_\gamma}{c}\right)\frac{l}{\hbar}\right\}$$

A is the area of a Unit Cell

$$\boldsymbol{J}_i(\boldsymbol{r}) = \frac{-e}{m^*(2\pi)^2}\sum_{\alpha\sigma}\int_{-\pi}^{\pi} d\boldsymbol{\theta}\, \text{Re}\{\psi^*_{\alpha\theta\sigma}(\boldsymbol{r})\boldsymbol{\pi}_i\psi_{\alpha\theta\sigma}(\boldsymbol{r})\} \times f(E_{\alpha\theta\sigma} - \mu),$$

$$n_{\text{e}}(\boldsymbol{r}) = \frac{1}{(2\pi)^2}\sum_{\alpha\sigma}\int_{-\pi}^{\pi} d\boldsymbol{\theta}\, |\psi_{\alpha\theta\sigma}(\boldsymbol{r})|^2 f(E_{\alpha\theta\sigma} - \mu)$$

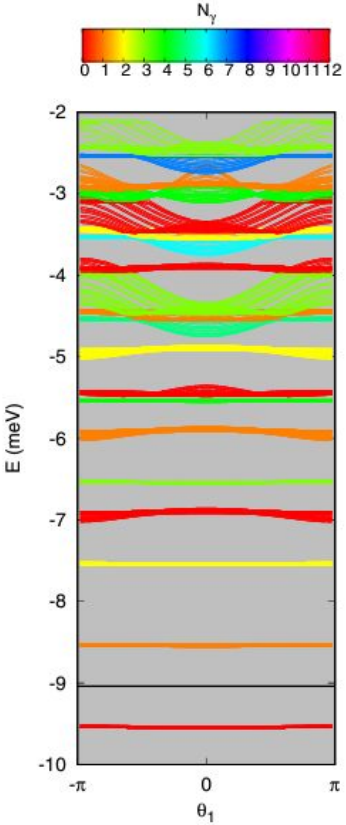

FIG. 1. The energy band structure projected on the θ_1 direction in the first Brillouin zone for $N_e = 2$ and $pq = 2$ (two flux quanta) corresponding to $B \approx 0.827$ T. The color of the bands indicates their photon content with red for 0 and violet for 12. The color scale is at the top of the figure. The chemical potential μ is shown by the horizontal black line. Due to the low magnetic field, the spin splitting of the bands is not clearly visible on the energy scale used. $E_\gamma = \hbar\omega_\gamma = 1.00$ meV, $g_\gamma = 0.001$, $L = 100$ nm, and $T = 1$ K.

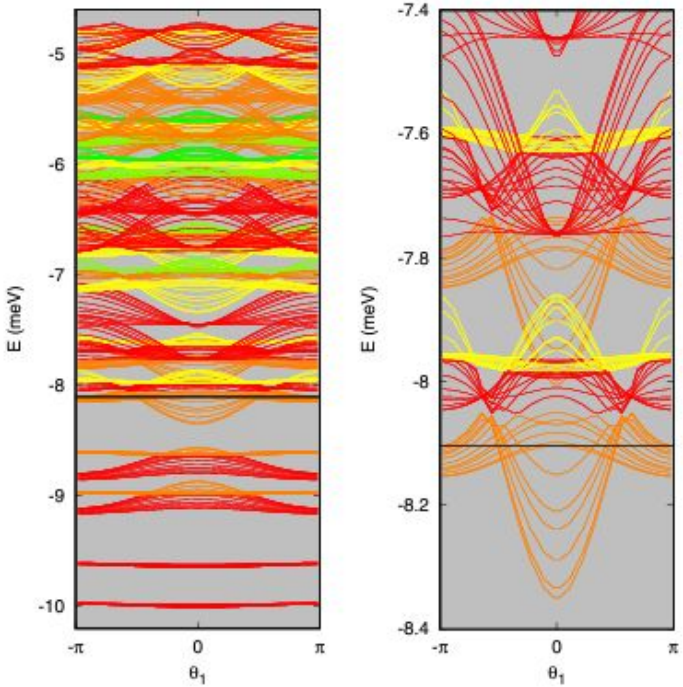

FIG. 5. The energy band structure projected on the $\theta_1 = k_1 L$ direction in the first Brillouin zone for $N_e = 7$, and $pq = 2$ (left) and a section of the same band structure in an energy range around the chemical potential (right). The color of the bands indicates their photon content with red for 0 and violet for 12. The chemical potential μ is shown by the horizontal black line. The color scale is the same as in Fig. 1. An enhanced spin splitting of the bands is seen. $E_\gamma = \hbar\omega_\gamma = 1.00$ meV, $g_\gamma = 0.005$, $L = 100$ nm, and $T = 1$ K.

QD array

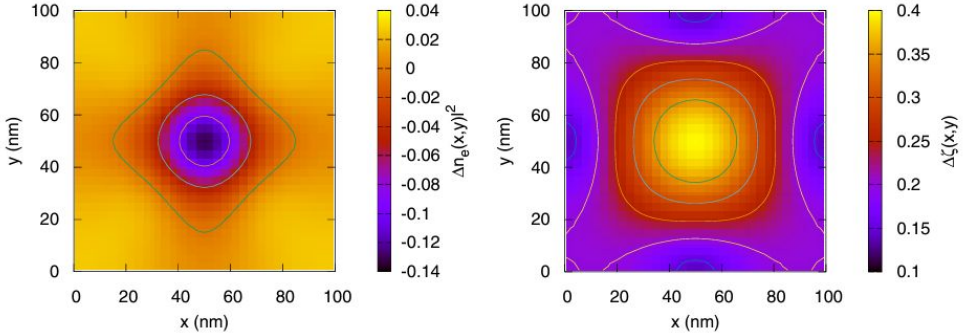

FIG. 7. The change in the electron density $n_e(x, y)$ (left), and the electron spin polarization $\zeta(x, y)$ (right) when the dimensionless electron-photon coupling constant g_γ is changed from 0.005 to 0.750. $N_e = 7$, $pq = 2$, and $E_\gamma = 1.0$ meV. $L = 100$ nm, and $T = 1$ K.

QR array

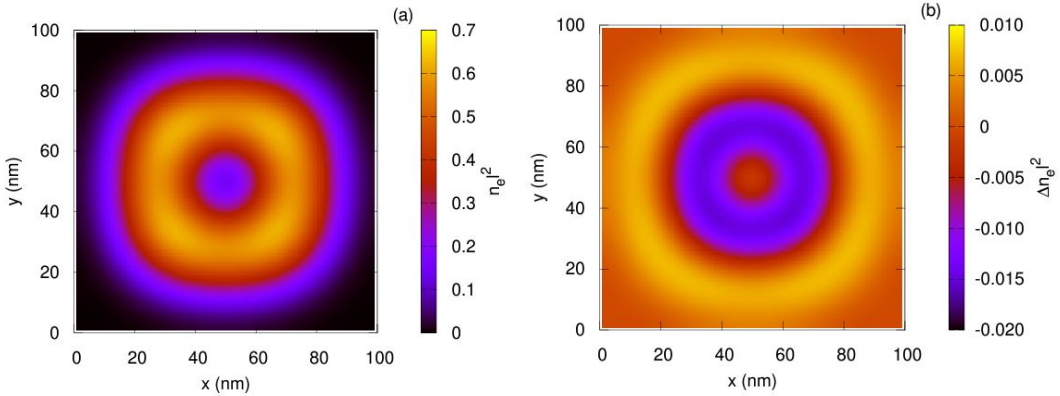

FIG. 5. The electron density $n_e l^2$ (a), the change in the electron density $\Delta n_e l^2 = [n_e(g_\gamma = 0.10) - n_e(g_\gamma = 0.01)]l^2$ (b),

QD array

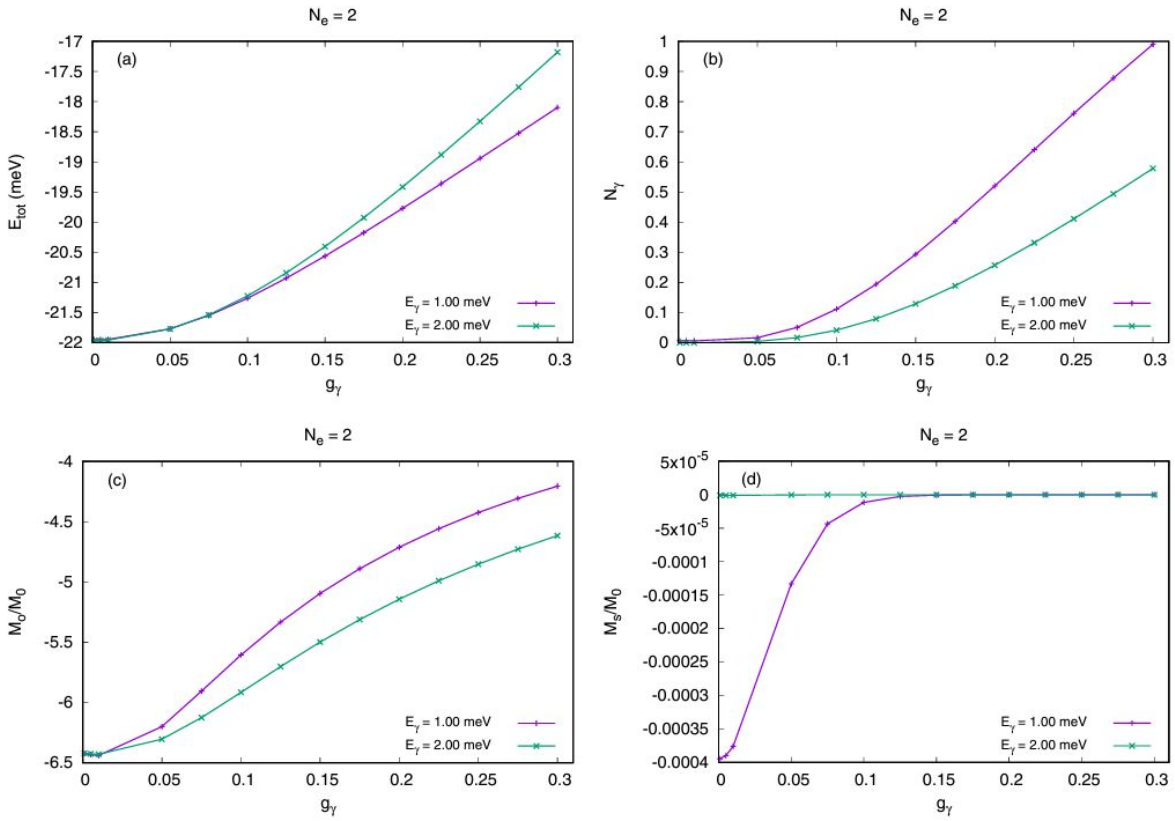

FIG. 2. The total energy (a), the mean number of photons (b), the orbital magnetization (c), and the spin magnetization (d) as functions of the dimensionless electron-photon coupling constant g_γ for $N_e = 2$, and $pq = 2$. $L = 100$ nm, $T = 1$ K, and $M_0 = \mu_B^*/L^2$.

QR array

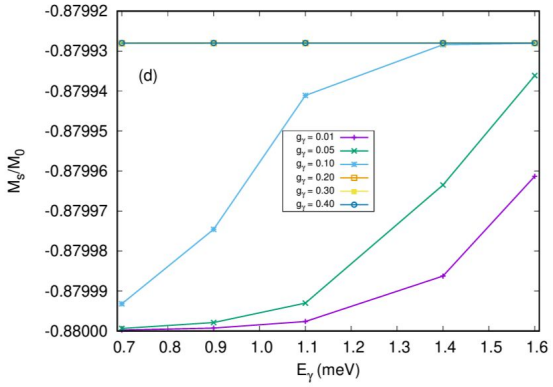

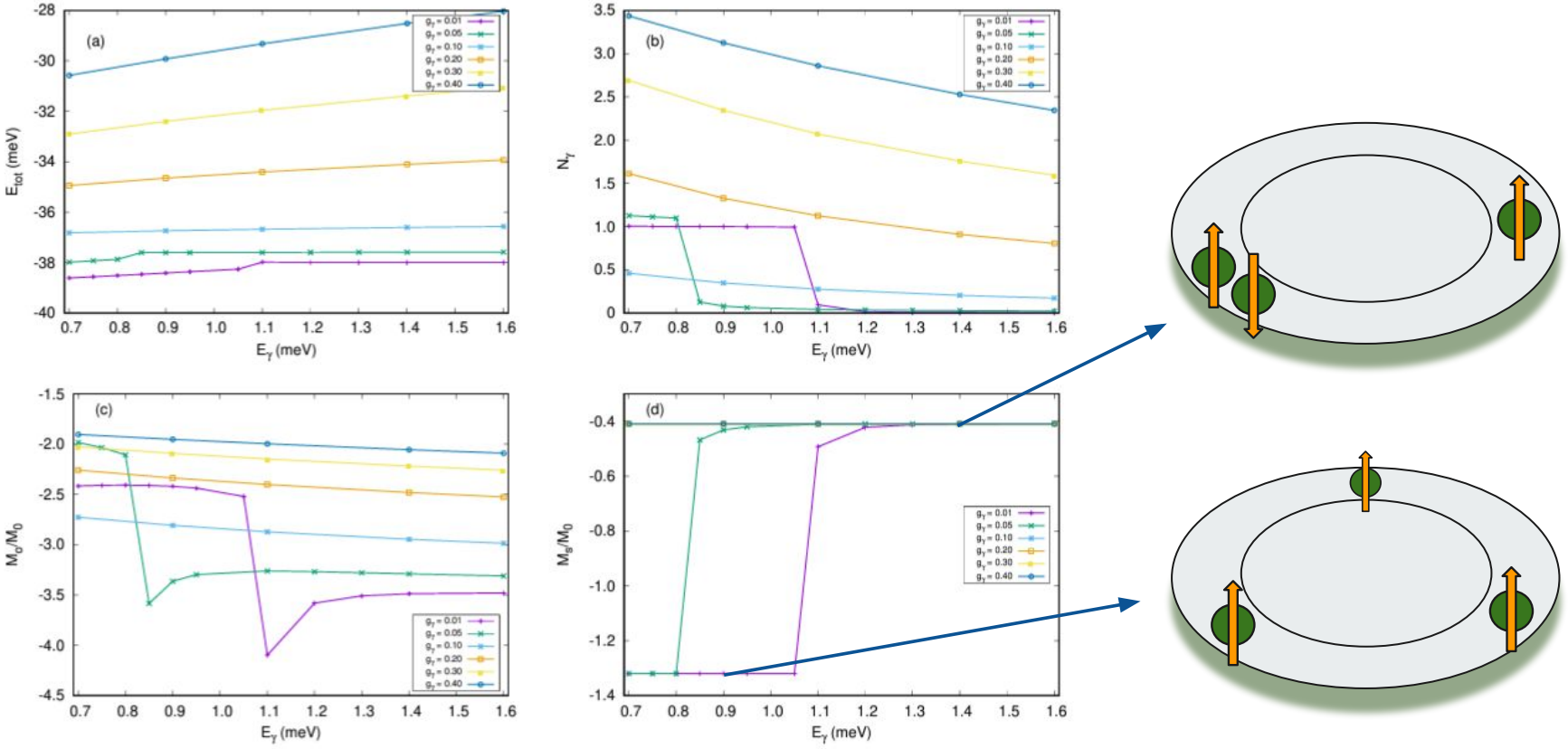

FIG. 6. The total energy $E_{\rm tot}$ (a), the mean number of photons N_γ (b), the orbital magnetization M_o (c), and the spin magnetization M_s (d) of the 2DEG in a unit cell as function of the photon energy E_γ for different values of the dimensionless electron-photon coupling g_γ. $T = 1.0$ K, $N_{\rm e} = 3$, $pq = 2$, $M_0 = \mu_{\rm B}^*/L^2$.

In order to explore the dynamical evolution of the system, it is excited with a short pulse-like modulation of the electron-photon interactions.

$$H_{\text{ext}}(t) = F(t)\Big[g_\gamma \hbar\omega_c \left\{lI_x + lI_y\right\}\left(a_\gamma^\dagger + a_\gamma\right) \tag{9}$$
$$+ g_\gamma^2 \hbar\omega_c \mathcal{N}\left\{\left(a_\gamma^\dagger a_\gamma + \frac{1}{2}\right) + \frac{1}{2}\left(a_\gamma^\dagger a_\gamma^\dagger + a_\gamma a_\gamma\right)\right\}\Big]$$

with

$$F(t) = \left(\frac{V_t}{\hbar\omega_c}\right)(\Gamma t)^2 \exp\left(-\Gamma t\right)\cos\left(\omega_{\text{ext}} t\right). \tag{10}$$

The time-evolution of the system is calculated self-consistently with the Liouville-von Neumann equation for the density, or the probability, operator $\rho^{\boldsymbol{\theta}}(t)$ for each $\boldsymbol{\theta}$-point in the first Brillouin zone of the reciprocal lattice.

$$i\hbar\partial_t \rho^{\boldsymbol{\theta}}(t) = \left[H[\rho^{\boldsymbol{\theta}}(t)], \rho^{\boldsymbol{\theta}}(t)\right]. \tag{11}$$

$\hbar\omega_{\text{ext}} = 3.5$ meV, $\hbar\Gamma = 0.5$ meV, and $V_t/\hbar\omega_c = 0.8$

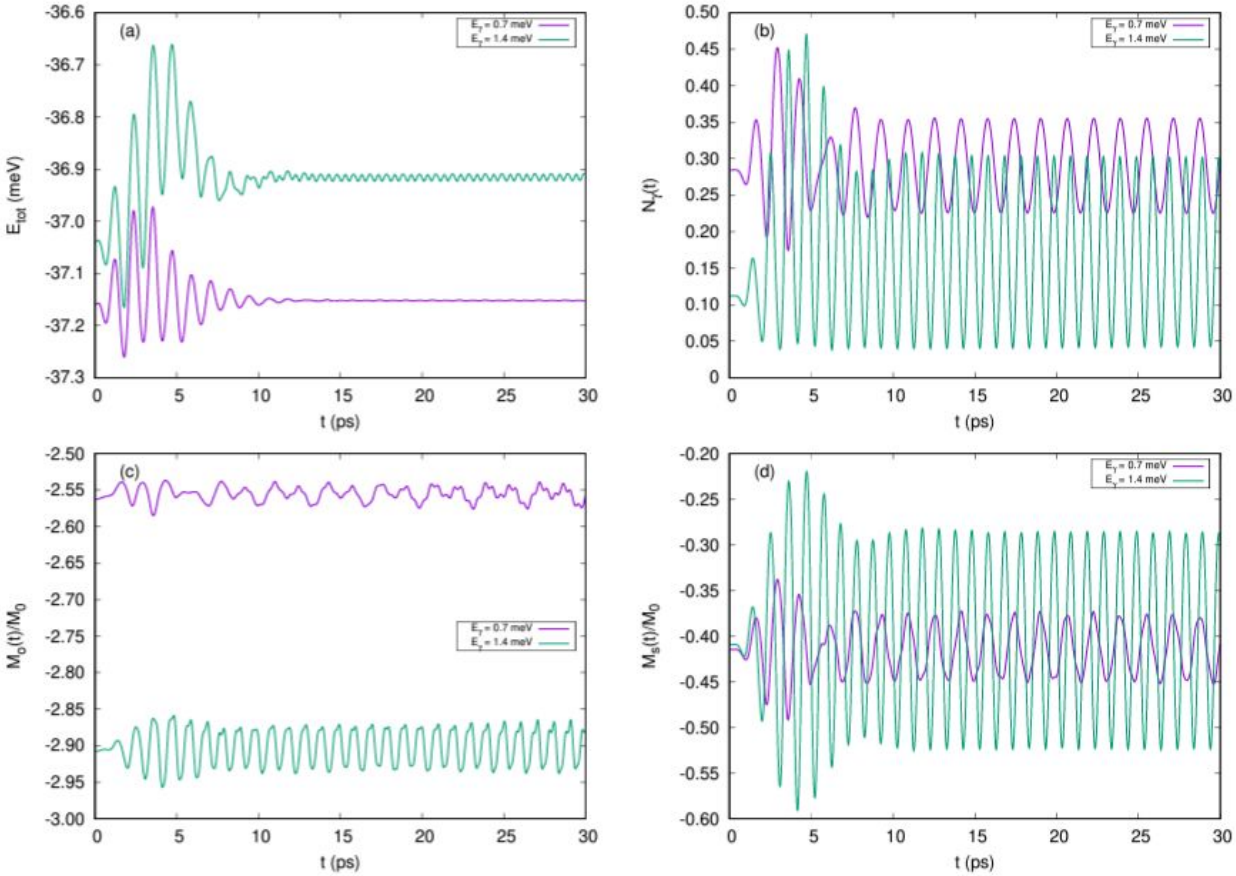

FIG. 7. The total energy $E_{\rm tot}$ (a), the mean number of photons N_γ (b), the orbital magnetization M_o (c), and the spin magnetization M_s (d) of the 2DEG in a unit cell as function of time for the first 30 ps for different values of the photon energy E_γ. $g_\gamma = 0.08$, $N_{\rm e} = 3$, $pq = 2$, and $M_0 = \mu_{\rm B}^*/L^2$.


NÁTTÚRULEGT
KOFFÍN
COLLAB

NanoSM
Center for Modeling and Simulations

ԵՐԵՎԱՆԻ ՊԵՏԱԿԱՆ ՀԱՄԱԼՍԱՐԱՆ

ՀՀ կրթության, գիտության, մշակույթի և սպորտի նախարարություն
RA MESCS HIGHER EDUCATION AND SCIENCE COMMITTEE

Շնորհակալություն

Thank You !

rannís

A. ALIKHANYAN
National Laboratory